Structural Features of Alveolar Wall Basement Membrane in the Adult Rat Lung

CHARLES A. VACCARO and JEROME S. BRODY
Pulmonary Section, Departments of Medicine, Boston City and University Hospitals, Boston University School of Medicine, Boston, Massachusetts 02118

ABSTRACT The ultrastructural characteristics of alveolar (ABM) and capillary (CBM) basement membranes in the adult rat lung have been defined using tannic acid fixation, ruthenium red staining, or incubation in guanidine HCl. ABM is dense and amorphous, has 3- to 5-nm filaments in the lamina rara externa (facing the alveolus) that run between the lamina densa and the basal cell surface of the epithelium, has an orderly array of ruthenium red-positive anionic sites that appear predominantly (79%) on the lamina rara externa, and has discontinuities beneath alveolar type II cells but not type I cells that allow penetration of type II cytoplasmic processes into the interstitium of the alveolar wall. The CBM is fibrillar and less compact than ABM, has no lamina rara filaments, and has one fifth the number of ruthenium red-positive anionic sites of ABM that appear predominantly (64%) overlying the lamina densa. Incubation of lung tissue with *Flavobacterium heparinum* enzyme or with chondroitinase has shown that ABM anionic sites represent heparan sulfate proteoglycans, whereas CBM anionic sites contain this and other sulfated proteoglycans. The CBM fuses in a focal fashion with ABM, compartmentalizing the alveolar wall into a thick and thin side and establishing a thin, single, basement-membrane gas-exchange surface between alveolar air, and capillary blood. The potential implications of ABM and CBM ultrastructure for permeability, cell differentiation, and repair and morphogenesis of the lung are discussed.

Basement membranes[1] are heterogeneous structures that serve to delineate boundaries and to compartmentalize tissues. They act as scaffolds guiding morphogenesis (1) and tissue repair (2), and they also play a role in regulating permeability of macromolecules (3) and in modulating movement of cells (4). Despite tbe obvious relevance of all of these functions to the lung, the fine structure of the basement membranes in the alveolar wall of the lung has not been well defined.

The structure of the alveolar wall was not characterized in detail until the early electron microscopy studies of Low and Karrer (5, 6). Much of this early work was concerned with describing the general arrangement of cells in the alveolar wall. Subsequent studies concentrated on the alveolar interstitium, defining a thin and thick side of tbe alveolus and describing an alveolar and a capillary basement membrane (7–9). These studies emphasized the similarity of alveolar and capillary basement membranes, both of which appeared as homogeneous bands of low electron density. Recent immunocytochemical studies have supported this similarity since both basement membranes contain types IV and AB_2 collagen (10).

The wall of the pulmonary alveolus has been shown to consist of a thin side, where capillary endothelium and alveolar epithelium are separated only by basement membrane, and a thick side, where endothelium and epithelium are separated by their respective basement membranes and by the connective tissue of the interstitial space (11). Capillaries wind back and forth across the alveolar wall, creating alternating thick and thin sides. Since individual ABM and CBM cannot be seen on the thin side it has been assumed that the two basement membranes fuse in this area (8, 9). This view has been supported by a recent study that found separate identifiable ABM

[1] Throughout this paper the term basement membrane will refer to the whole of the collagenous and noncollagenous structure immediately beneath alveolar epithelium or capillary endothelium that is defined by our staining methods. Thus, basement membrane, as used here, includes basal lamina, associated proteoglycans, and other as yet incompletely defined components. The basement membrane below alveolar type I and type II cells will be referred to as alveolar basement membrane (ABM) and that below capillary endothelial cells will be referred to as capillary basement membrane (CBM).

THE JOURNAL OF CELL BIOLOGY · VOLUME 91 NOVEMBER 1981 427–437
© The Rockefeller University Press · 0021-9525/81/11/0427/11 $1.00

and CBM in close proximity on the thin side of the alveolus in specimens of human lung which had been incubated in guanidine HCl (12).

We have previously shown that incubation of lung tissue with ruthenium red allows ultrastructural definition of ABM and visualization of ABM-associated proteoglycans (13). In this paper we present the results of our studies of ABM and CBM in the adult rat lung, employing a variety of additional techniques that emphasize basement membranes and their components. We have found that ABM and CBM have different ultrastructural characteristics; that they are both closely associated with proteoglycans, although the distribution and type of these proteoglycans differs in the two basement membranes; and that, in contrast to previous reports, fusion between ABM and CBM does not extend the length of the thin side of the alveolar wall but that it is focal in nature, forming basement-membrane-delineated vascular and extravascular compartments within the lung.

MATERIALS AND METHODS

Tannic Acid Fixation

Sprague-Dawley rats, 250–300 g, were killed by intraperitoneal injection of 2 mg of pentobarbital/100 g of body weight. The trachea was exposed and cannulated and lungs were inflated at 25–30 cm H_2O pressure with 1% tannic acid and 1% glutaraldehyde in 0.075 M phosphate buffer, pH 7.2–7.3. The chest cavity was opened and random samples of each lobe were excised, cut into 1- to 2-mm cubes, and placed in fresh fixative for 2–3 h at room temperature. After tannic acid/glutaraldehyde fixation, tissues blocks were washed four times over 10 min with 0.075 M phosphate buffer containing 0.18 M sucrose. The tissue was postfixed for 1–2 h in osmium in phosphate buffer with sucrose at room temperature. After osmication, the tissue was quickly rinsed in two changes of phosphate buffer and rapidly processed (14) through ascending concentrations of ethanol or acetone. Blocks were infiltrated in a Polybed 812-Araldite 502-DDSA-DMP-30 mixture split 50:50 with acetone for 20 min on a standard rotor. Rapid processing involved two additional changes with 100% resin mixture for 30 min each on the rotor. The blocks were embedded in fresh resin and polymerized at 60°C for 1–24 h. Before thin sectioning, the plastic was further polymerized by heating for 1 h at 100°C. Routine thin sections were obtained with glass or diamond knives and stained with uranyl acetate and lead citrate. Electron micrographs were prepared with a Philips EM 300 electron microscope.

Karnovsky Fixation

Additional animals were sacrificed and the lungs were inflated with a one-quarter-strength glutaraldehyde/paraformaldehyde mixture (15) buffered with 0.2 M Na cacodylate, pH 7.2–7.3. Samples of each lobe were cut and placed in fresh fixative for an additional 2–4 h at room temperature. The blocks were rinsed in four 5-min changes of 0.2 M cacodylate buffer and postfixed in osmium tetroxide buffered with Na cacodylate for 1–2 h. Tissue samples were rapidly processed through acetone and embedded in plastic using the method described under Tannic Acid Fixation.

Guanidine HCl

Unfixed blocks of lung tissue were placed in a 5 M guanidine hydrochloride solution (pH 7.0–7.1) at room temperature for 24 h. On the next day, blocks were washed with 0.075 M phosphate buffer plus 0.18 M sucrose and processed for electron microscopy with the tannic acid fixation regimen described above.

Ruthenium Red Staining

Adult rat lungs were gently inflated with 1% Triton X-100 and 1% ruthenium red mixture in McIlvaine's buffer, pH 5.6. Triton X-100 will severely damage the lung parenchyma but allows the ruthenium red to penetrate the lung interstitium and stain the basement membrane and collagen proteoglycans (13). Samples of the whole lung were incubated in the buffered detergent with ruthenium red for 1 h with gentle agitation. The tissue was fixed in 5% glutaraldehyde plus 1% ruthenium red in McIlvaine's buffer overnight at 4°C. On the next day, the blocks were washed four times for 5 min each with fresh buffer containing ruthenium red, and postfixed for 1–2 h in 1% osmium tetroxide in McIlvaine's containing 0.75% ruthenium red. After postfixation, the tissue was rinsed twice with buffer and rapidly processed for electron microscopy.

Characterization of Basement-membrane Anionic Sites

To identify the specific character of ruthenium-red granules associated with lung basement membranes, we incubated minced pieces of perfused lung in chondroitinase ABC, crude heparanase, or phosphate-buffered saline before staining with ruthenium red. Chondroitinase ABC (Miles Laboratories Inc., Elkhart, Ind.) was used at a concentration of 1 U/ml in enriched Tris buffer (pH 8.0). This enzyme is known to selectively degrade dermatan and chondroitin 4 and 6 sulfate glycosaminoglycans (16). Heparanase (kindly supplied by Dr. J. E. Silbert, Boston, Mass.) is prepared from *Flavobacterium heparinum* and was used at a concentration of 2 U/2.5 mg of protein lung tissue at pH 7.0 (17). The enzyme contains chondroitin lyase, dermatanase, heparinase, and heparanase activity and thus will degrade sulphated glycosaminoglycans (17). Control and enzyme-treated lung pieces were incubated at 37°C for 30 min. After enzyme digestion, the tissue samples were stained with ruthenium red as outlined under Ruthenium Red Staining, except that Triton X-100 was eliminated, and then were processed routinely for electron microscopy (Tannic Acid Fixation).

Morphometry of Type II Cell Basilar Processes and of Basement-membrane Anionic Sites

Tissue samples from lungs of two animals fixed with tannic acid as described above and processed for electron microscopy were used for Type II cell morphometry. 25 pictures of type II cells were taken at random from grids prepared from four different blocks, and prints were enlarged to a standard magnification. We counted the number of basilar cytoplasmic processes in each type II cell and the number of times these processes penetrated the type II cell basement-membrane lamina densa. Tissue samples of three lungs were stained with ruthenium red as described above and processed routinely for electron microscopy. 20 pictures per animal were taken, at random, of the alveolar and capillary basement membranes. All negatives were enlarged to the same print magnification to count ruthenium red–positive sites. Areas of basement membrane that were tangentially sectioned were not counted. We measured the length and counted the total number of granules associated with the ABM and CBM present in each micrograph. The total number of sites on either side and in the center of the lamina densa associated with the epithelial lamina were separately counted and recorded.

RESULTS

General Structure

The general architecture of the alveolar wall is illustrated in Fig. 1*a*. The thin side of the alveolar wall, where diffusion distances for gases are minimal, is formed by the close approximation of capillary endothelium and alveolar epithelium, the two being separated only by basement membrane. The thick

FIGURE 1 (*a*) Tannic acid fixation of alveolar wall, which consists of a thin side with alveolar basement membrane (*ABM*) separating type I cell epithelium (*Ep*) and endothelium (*En*) and a thick side with capillary basement membrane (*CBM*) separated from ABM by interstitial collagen (*col*) and elastin (*el*). An alveolus (*ALV*) lies on either side of the alveolar wall. Bar, 1.0 μm. × 13,887. (*b*) The alveolar basement membrane contains a distinct lamina rara (*LRI*) region. Filaments (arrows) in the lamina rara externa (*LRE*) connect the lamina densa (*LD*) component to the basal epithelial cell surface. Bar, 0.1 μm. × 116,072. (*c*) The lamina densa of the capillary basement membrane is more fibrillar (arrow), and filaments do not appear in the externa region. Bar, 0.1 μm. × 109,725. (*d* and *e*) After conventional fixation in glutaraldehyde and paraformaldehyde, the ABM and CBM appear amorphous and form continuous bands between epithelial (*Ep*) and endothelial (*En*) cell surfaces. Bar, 0.1 μm. × 109,725.

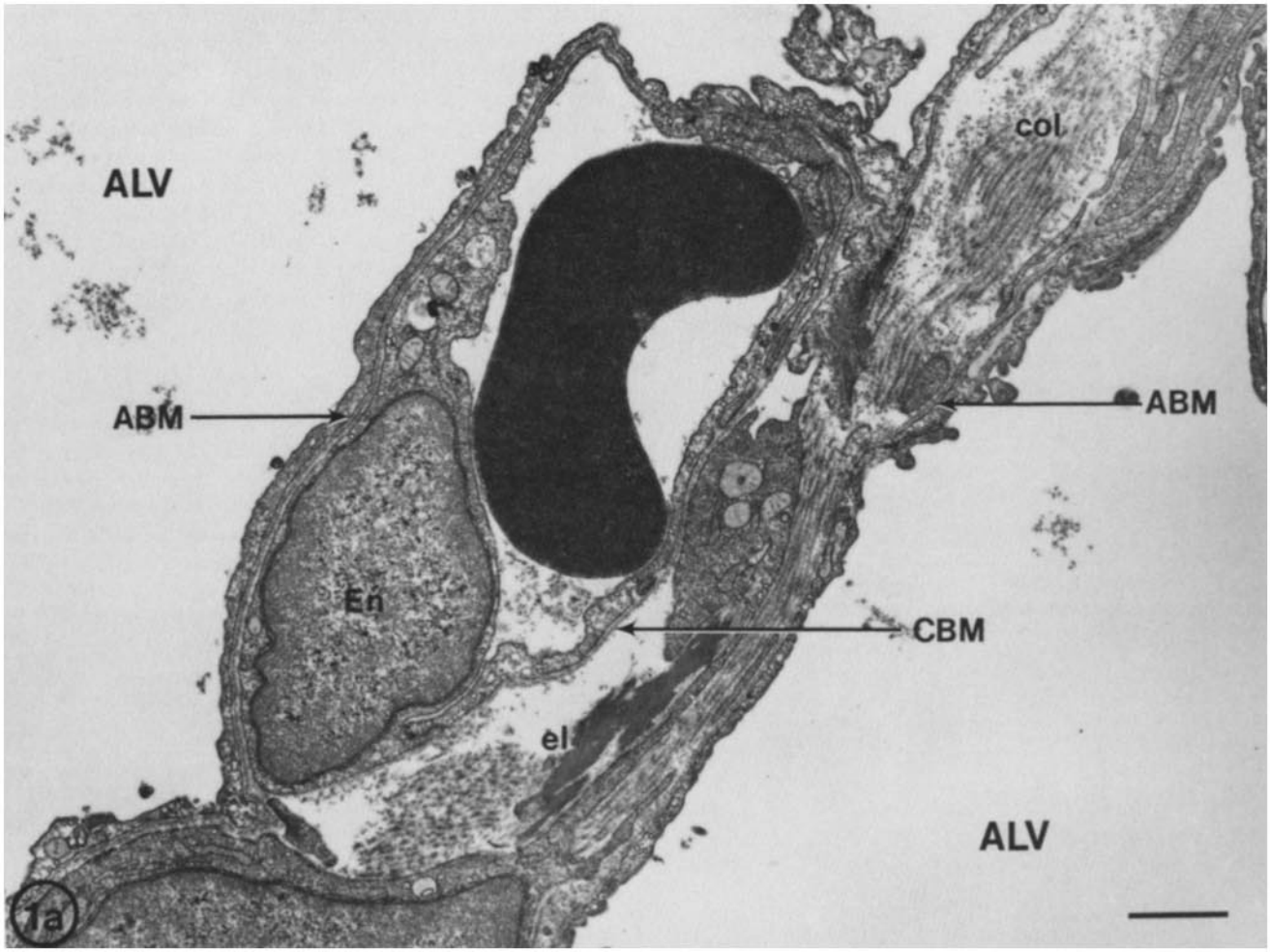
ALV
col
ABM
ABM
En
CBM
el
ALV
1a

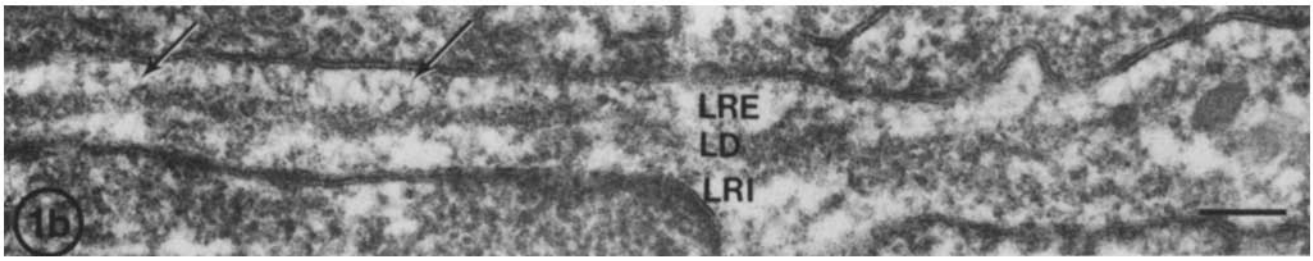
LRE
LD
LRI
1b

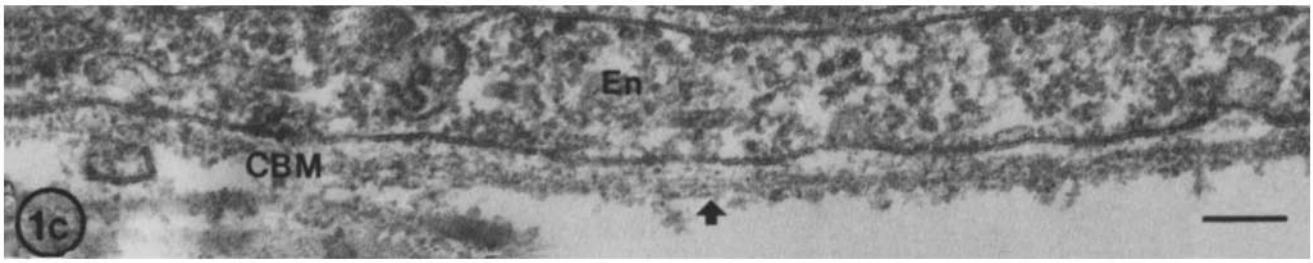
En
CBM
1c

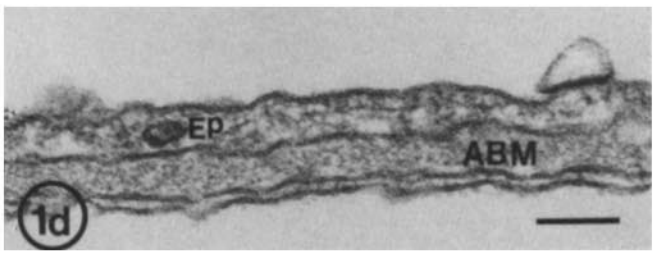
Ep
ABM
1d

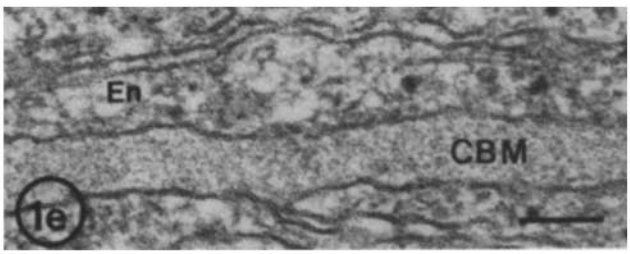
En
CBM
1e

side of the alveolar wall consists of collagen, elastin, and other matrix materials that, together with interstitial cells, separate endothelium and epithelium and their distinct basement membranes.

Conventional fixation and staining reveals amorphous bands of ABM and CBM that appear to be similar in structure (Fig. 1 *d* and *e*). Fixation with tannic acid (Fig. 1 *b* and *c*) illustrates ABM and CBM lamina densa and lamina rara and shows the lamina densa of each to be of similar thickness, although tannic acid also accentuates several differences between basement membranes. The lamina densa of the CBM has a more fibrillar appearance than that of the ABM, a difference also noted with other staining techniques. Ruthenium red not only stains anionic sites on each basement membrane (see below) but also emphasizes the fibrillar nature of the CBM lamina densa. The CBM lamina densa consists of thin threadlike fibrils that at times are arranged in parallel rows and at times are interconnected, giving the lamina a netlike appearance. The difference in ABM and CBM lamina densa is accentuated by exposure to Triton X-100 before staining with ruthenium red. This produces a lacy appearance in CBM but does not significantly change the homogeneous ABM. The fibrillar vs. dense contrast of CBM and ABM is also accentuated by incubation with guanidine hydrochloride.

TABLE I

Type II Cell Basilar Foot Processes (FP)

Measure	$\bar{X} \pm$ SEM
FP/cell	2.9 ± 0.7
FP penetrating ABM/cell	0.7 ± 0.4
% Cells with FP	68
% Cells with FP penetrating ABM	32

Filaments

Numerous 5- to 10-nm filaments lie in the lamina rara externa of the ABM running in a perpendicular fashion between the ABM lamina densa and the basal cell surface of tbe overlying epithelium (Fig. 1 *b*). These filaments appear less distinct in the lamina rara interna of the ABM and do not appear to be present in tbe laminae rarae of the CBM. Patches of amorphous material appear in the laminae rarae of the CBM

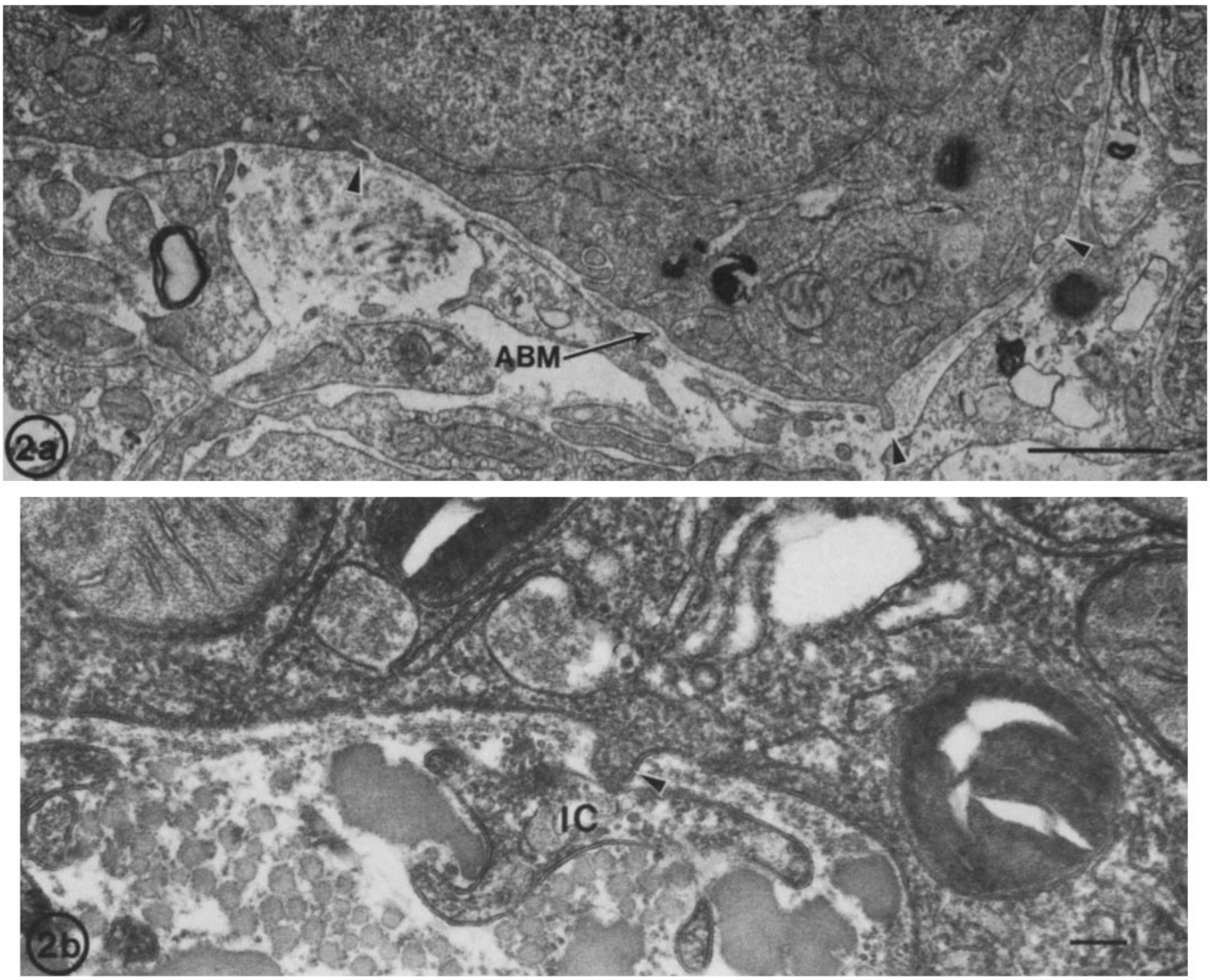

FIGURE 2 (*a* and *b*) The basal cell membrane of type II cells displays cytoplasmic extension (arrowheads) that can penetrate the alveolar basement membrane (*ABM*) and appear in close approximation to interstitial cells (*IC*). (*a*) Bar, 1 μm; × 21,141. (*b*) Bar, 0.1 μm; × 85,120.

and lamina rara interna of the ABM, but these differ from the above noted filaments.

Basement Membrane–penetrating Cytoplasmic Processes

Numerous short cytoplasmic processes (foot processes) exist on the basal surface of alveolar type II cells: an average of 2.9/cell (Table I). Approximately 25% of these foot processes (0.7/cell) penetrate the ABM lamina densa and extend into the interstitium of the alveolar wall (Fig. 2 *a* and *b*). These type II cell cytoplasmic extensions often appear in close proximity to interstitial fibroblasts but in no instance do they form clear junctions with these cells. No such foot processes are seen beneath alveolar type I cells or endothelial cells, and no discontinuities exist in the ABM or CBM beneath these cells.

Distribution of Basement-membrane Anionic Sites

When stained with ruthenium red, ABM lamina densa is compact, structurally amorphous, and contains numerous anionic sites that bind the cationic dye ruthenium red (Fig. 3 *a*). The ruthenium red–positive granules are localized predominantly at the surface of lamina densa. Viewed in cross section, more granules are localized to the surface facing the lamina rara externa region (Fig. 3 *b*). Areas of basement membrane sectioned in a tangential plane (Fig. 3 *d*) and sectioned through the surface of the lamina rara externa (Fig. 3 *e*) illustrate that the anionic sites are evenly distributed and form a three-dimensional sheet with a distance between anionic sites of 55–65 nm.

The distribution of ruthenium red–positive anionic sites is different in the CBM (Fig. 3 *a* and *c*). Most of the CBM anionic sites appear in the lamina densa, with only 35% of sites appearing in the two laminae rarae (Table II). Furthermore, CBM contains approximately one fifth the number of sites seen in the ABM. This pattern is more consistent with anionic sites winding around or through the CBM rather than lying on a surface, as is the case with the ABM.

Nature of Basement-membrane Anionic Sites

To determine the chemical nature of these anionic sites we treated lung tissue with a series of glycosaminoglycan-degrading enzymes. Figs. 4 and 5 represent a series of micrographs of the ABM and CBM incubated in buffer, chondroitinase ABC, or *Flavobacterium heparinum* enzyme before staining with ruthenium red. The ruthenium red–positive granules remain intact along the ABM (Fig. 4 *b*) after digestion with chondroitinase ABC. Compared wth control specimens, the granules retained their shape, were periodically spaced, and localized predominantly at the densa to externa surface. After digestion with *F. heparinum* enzyme both the surface and matrix granules were removed (Fig. 4 *c*), indicating that the predominant glycosaminoglycan present on the ABM is heparin and/or heparan sulfate. Further identification of this material will be presented elsewhere. Previous studies have demonstrated that the ABM-associated granules are resistant to enzymes that degrade hyaluronic acid, dermatan sulfate, and chondroitin 4 and 6 sulfates (13). On the other hand, chondroitinase appeared to exhibit some activity against granules present in CBM (Fig. 5 *b*). Although several deposits remain clearly visible after chondroitinase digestion, compared to control samples, the granules are smaller and fewer in number. Digestion with *F. heparinum* enzyme is less selective and removes all the granules, leaving the fibrillar matrix intact (Fig. 5 *c*). Thus, CBM contains a mixture of sulfated proteoglycans with larger amounts of heparan sulfate intermixed with dermatan and/or chondroitin 4 or 6 sulfate.

Basement Membrane Fusion

Fig. 6 illustrates points of fusion between the alveolar and the capillary basement membrane in lung specimens fixed with tannic acid, treated with guanidine hydrochloride, or stained with ruthenium red. Under these different conditions, fusions consistently occur in a focal or confined area at either end of the capillary. In tannic acid–fixed material, points of fusion appear to involve the coalescence of the epithelial and the endothelial lamina densa (Fig. 6 *a*). This coalescence produces a thickened or doubled lamina densa region that progressively thins until the basement membrane between the epithelial and endothelial cell surfaces contains a single rara interna and externa region.

After treatment with guanidine hydrochloride, the lung parenchyma is severely disrupted. Epithelial cells are lost, capillaries are distorted, and the ABM and CBM appear structurally different, with the CBM being more fibrillar in nature (Fig. 6 *b*). Points of fusion remain intact. As the area of fusion thins, only the amorphous epithelial lamina densa is visible, indicating that fusions do not extend the whole length of the thin side of the wall. Subjecting the lung to Triton X-100 before staining with ruthenium red significantly swells both the alveolar and the capillary basement membrane (Fig. 6 *c*). Points of fusion that merge into a single ABM are again illustrated. No specific structure appears at the fusion sites with any of the stains. There was no difference in the distribution of ruthenium red–positive granules between areas of fusion and other regions on the epithelial basement membrane (Fig. 6 *c*).

The results of our studies are summarized in a three-dimensional schema that illustrates the basement-membrane compartmentalization of the alveolar wall, the distribution of anionic sites, the structural differences between ABM and CBM, and the type II cell foot processes that penetrate the ABM (Fig. 7).

DISCUSSION

When viewed through the light microscope or with the usual fixatives and stains at an ultrastructural level, ABM and CBM of the alveolar wall appear similar in structure. However, with the various staining techniques used in our study we have been able to detect several differences between these two structures: (*a*) ABM has a dense, homogeneous, amorphous appearance, whereas CBM tends to be fibrillar in nature; (*b*) ABM and CBM react differently to detergent exposure; (*c*) ABM contains fine filaments in the lamina rara that are not seen in the CBM; (*d*) numerous discontinuities exist in the ABM beneath alveolar type II cells, whereas no discontinuities exist in the CBM; and (*e*) the distribution, density, and perhaps type of proteoglycans differ between the two structures.

CBMs tend to have a less dense, more fibrillar appearance when fixed with tannic acid or stained with ruthenium red than do ABMs. This fibrillar appearance is accentuated when lung tissue is incubated in guanidine HCl before fixation in tannic acid. Guanidine interacts with hydrophobic side chains of amino acid residues, thus denaturing proteins. Recently,

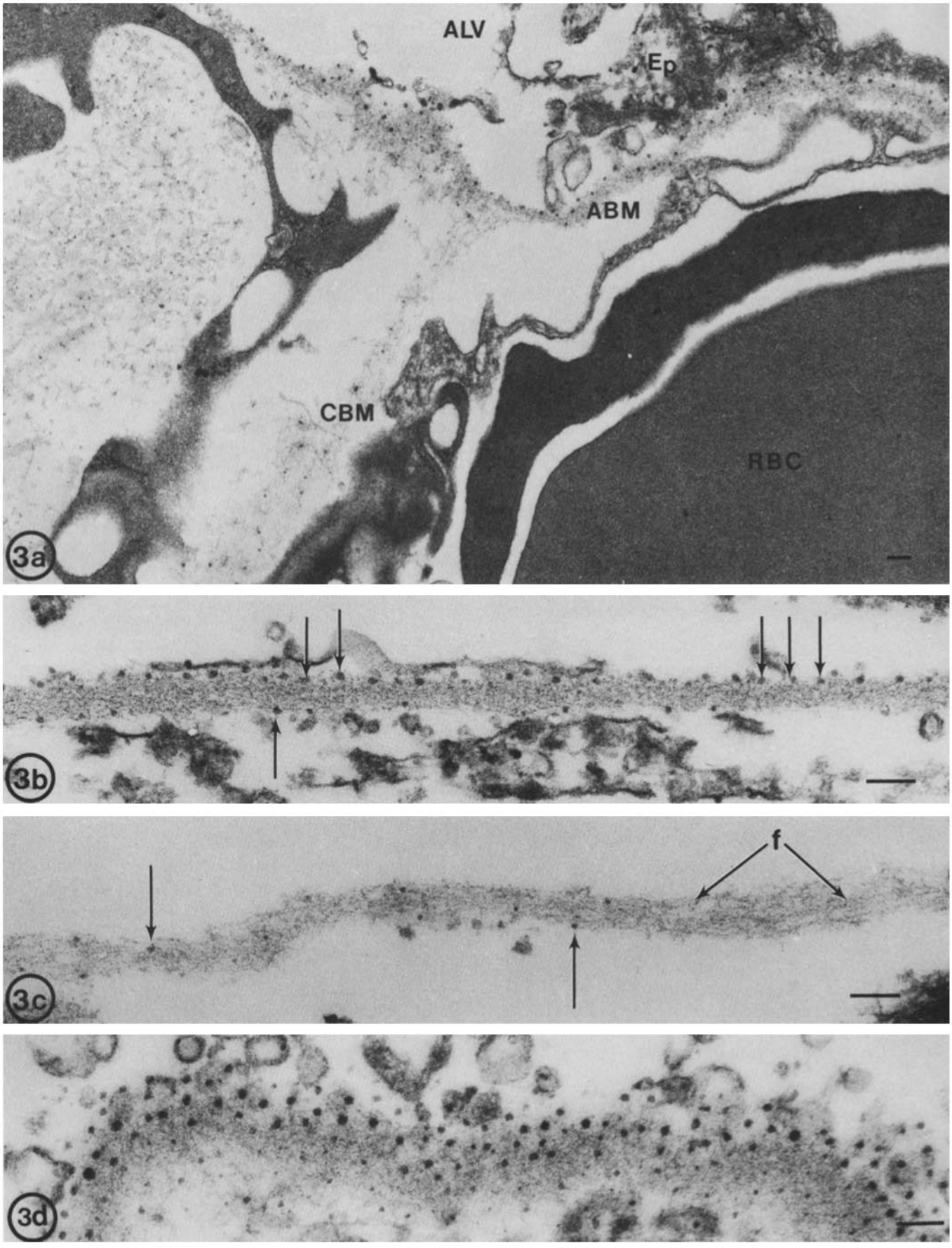
ALV
Ep
ABM
CBM
RBC
3a
3b
f
3c
3d

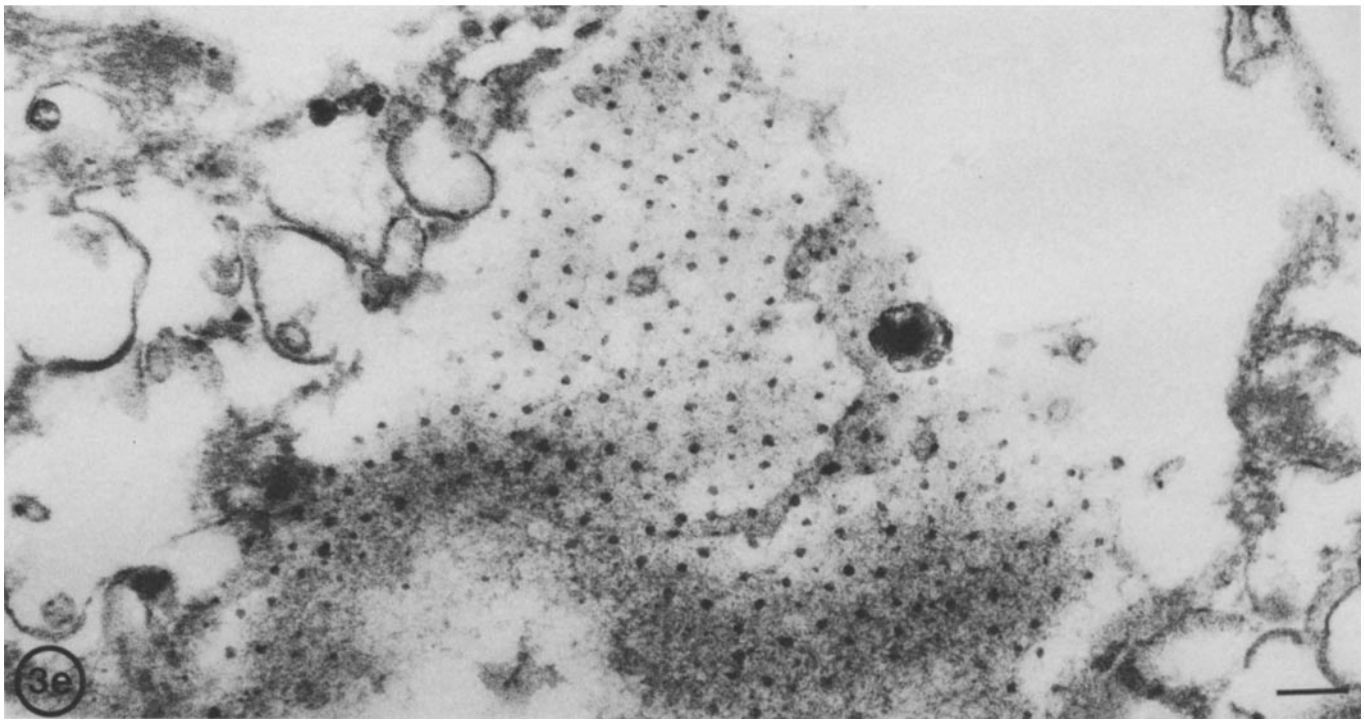

FIGURE 3 (a) Triton X-100 injures the alveolus (*ALV*) and fragments the surface epithelium (*Ep*). The alveolar and capillary basement membranes (*ABM* and *CBM*) remain intact and contain ruthenium red-positive granules. The capillary contains an erythrocyte (*RBC*). Bar, 0.1 μm. × 46,443. (*b*) Stained with ruthenium red, the ABM has an amorphous structure; anionic sites appear attached at the lamina densa surface (arrows) predominantly distributed along the surface facing the lamina externa region. Bar, 0.1 μm. × 92,858. (c) The capillary basement membrane contains fibrils (*f*) and fewer anionic sites (arrows) when stained with ruthenium red. Bar, 0.1 μm. × 95,858. (*d*) ABM viewed in a tangential plane suggests that granules are evenly space along the externa interface and are forming a three-dimensional sheet over the lamina densa. Bar, 0.1 μm. × 92,858. (*e*) ABM anionic sites viewed in longitudinal section through the lamina rara externa. Note the ordered arrangement of sites, with intersite distances of 55–65 nm. Bar, 0.1 μm. × 92,858.

TABLE II

Morphometric Analysis of Basement-Membrane Anionic Sites

	ABM	CBM
Distribution, %		
LRE	78.0	34.6
LRI	17.1	
LD	4.9	63.7
Anionic sites/100 nm, $\bar{X} \pm SEM$	2.17 ± 0.03	0.38 ± 0.02

LRE, lamina rara externa; *LRI*, lamina rara interna; *LD*, lamina densa. LRE and LRI could not be accurately distinguished in CBM and therefore are combined.

other chaotropic agents have been shown to denature fibronectin associated with collagen (18). Whether the guanidine-accentuated fibrillar vs. dense amorphous difference between CBM and ABM is attributable to differences in the amount and/or distribution of noncollagenous proteins such as fibronectin, or to differences in the cross-linking of the collagenous portion of each basement membrane, is unknown. The structural differences between ABM and CBM are also accentuated by incubation with the nonanionic detergent Triton. CBM appears to swell and becomes lacy in appearance, whereas ABM is unaltered. The reason for the Triton-induced change is uncertain but may relate to solubilization of noncollagenous substances that serve to link collagen molecules or to alterations in the polar environment of basement-membrane collagens.

Although the explanation of the above differences in ABM and CBM structure remains to be determined, it seems likely that the CBM is a more loosely organized structure and that it may be more permeable and more susceptible to disruption than the ABM. Kefalides (19) has recently reviewed the differences in amino acid composition and in the proportions of glycoprotein of the various basement membranes that have been isolated. Whether these relatively small differences can influence basement-membrane ultrastructure is not known. Further definition of the differences in collagen and noncollagen components of these two pulmonary basement membranes will likely require their isolation, separation, and chemical characterization.

Fine 3- to 5-nm filaments, seen best in tannic acid–fixed preparations, run perpendicularly from the ABM lamina densa to the cell plasma membrane of epithelial and endothelial cells; these filaments are not well seen in the CBM. The filaments appear similar to those that have been noted in glomerular basement membrane (20). Perfusion of kidney by the sialic acid–degrading enzyme, neuraminidase, leads to detachment of epithelial and endothelial cells from glomerular basement membrane with disappearance of filaments, suggesting that the filaments might serve a cell attachment function. Kanwar and Farquhar (21) have suggested that these filaments may represent fibronectin, which is known to contain sialic acid and to promote cell attachment and is present in most basement membrane studies to date (22). It is uncertain why filaments were seen on ABM but not on CBM. Fibronectin has been shown to complex with heparan sulfate proteoglycans, promoting cell-substrate adhesions (23, 24). The apparent differences in filament distribution between ABM and CBM may

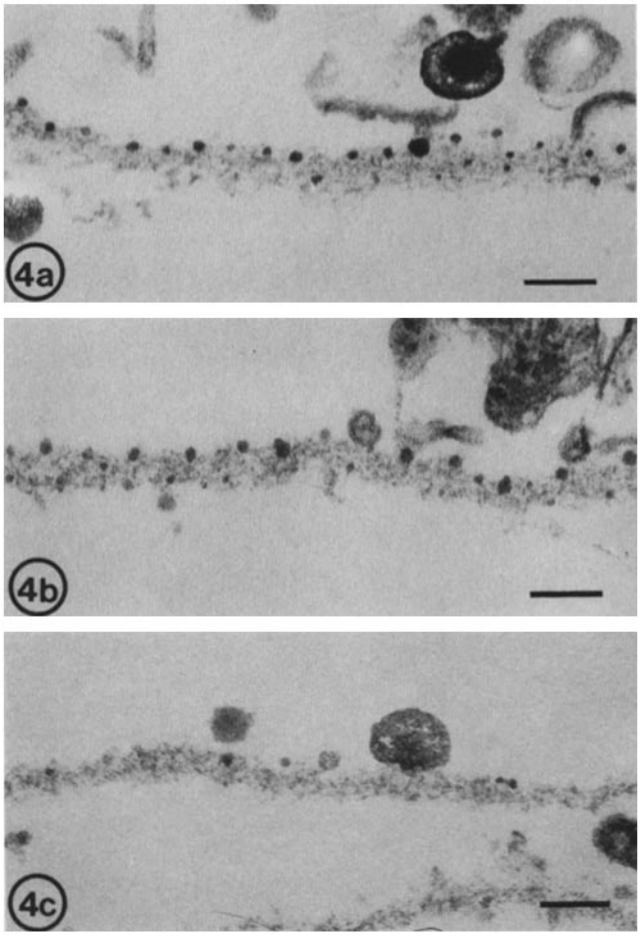

FIGURE 4 Compared with control samples (*a*) anionic sites associated with the alveolar basement membrane resist digestion with chondroitinase ABC (*b*). After incubation with *F. heparinum* enzyme (*c*), granules are removed from the lamina densa surfaces and within the matrix. Bar, 0.1 μm. × 88,989.

therefore relate to the differences in heparan sulfate proteoglycan distribution discussed below. It may be that the ABM-associated filaments represent a matrix glycoprotein other than fibronection. Laminin, another recently described basement membrane-associated glycoprotein, has been localized to the laminae rarae of epithelium and endothelium in a variety of organs including lung, although its specific distribution in ABM and CBM has not been determined (25, 26). Alternatively, these filaments might represent hyaluronic acid, which has a similar appearance in chick embryo fixed with tannic acid (27).

A major structural difference between ABM and CBM is the presence of discontinuities in the ABM that appear exclusively beneath alveolar type II cells. These discontinuities allow penetration of cytoplasmic processes from type II cells into the interstitium of the lung. On random thin sections, roughly two thirds of type II cells have basilar cytoplasmic processes with one third of the cells having processes that penetrate the basement membrane. When one considers that our 0.1 μm thin sections sample only a small portion of the surface of the type II cell, which is 70 μm^2 (28), it is likely that most if not all type II cells have multiple penetrating cytoplasmic processes. These cytoplasmic projections do not appear to form junctional complexes with interstitial cells although they frequently lie in close approximation to interstitial fibroblasts. Such epithelial-mesenchymal communications have been noted in many developing tissues including the fetal lung (29, 30). Most authors have attributed morphogenetic significance to these communications although recent studies have suggested that such epithelial-mesenchymal interactions may play a role in cytodifferentiation of epithelial cells (31, 32). We have found no ABM discontinuities or cytoplasmic extensions below type I cells, which are end-stage epithelial cells incapable of cell division (28, 33). The type II cell, in contrast, serves not only to produce the surfactant film that lines the alveolar surface but also, under conditions of rapid lung growth or lung repair after injury, can proliferate and differentiate into new type I cells (33, 34). It seems likely that the type II cell extensions we have noted are involved in controlling cytodifferentiation and function of this dual-potential cell. Recent studies have shown that fetal lung mesenchymal cells produce a low-molecular-weight peptide that stimulates synthesis of surfactant-associated phospholipids in fetal type II cells (35). Although no such studies have been done in the adult lung it is possible that these processes serve to modulate type II cell surfactant synthesis. It is also possible that the cytoplasmic processes allow accesses to hormones such as somatomedin C and corticosteroids that influence type II cell maturation (35, 37) or adrenergic agents which modulate surfactant secretion (38), thus providing a mechanism for control of type II cell function.

A final structural difference between ABM and CBM relates

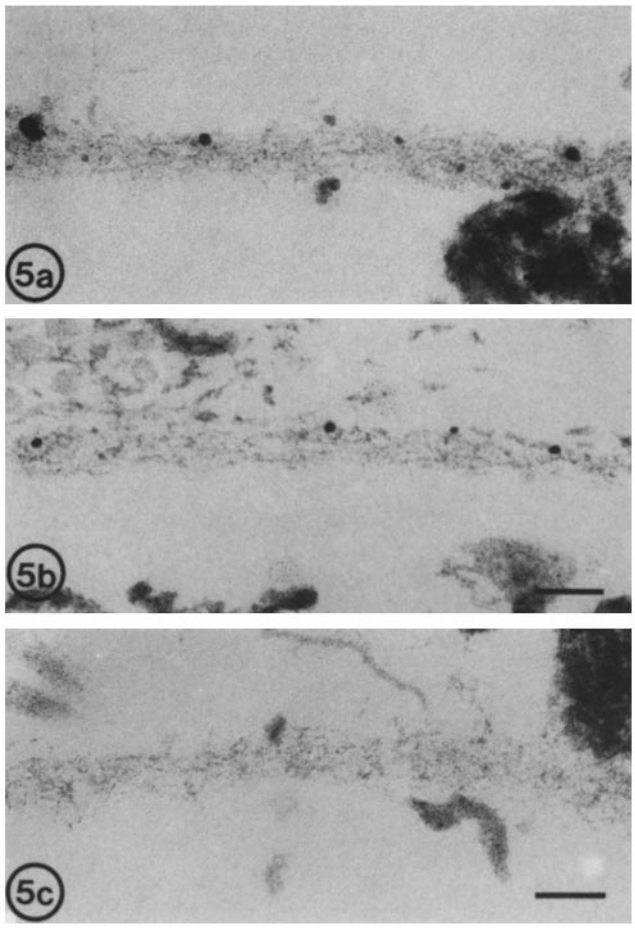

FIGURE 5 Ruthenium red-positive sites in capillary basement membrane from controls (*a*) appear partially lost after incubation with chondroitinase ABC (*b*) before staining. *F. heparinum* enzyme (*c*) completely removes the granules and leaves the fibrillar lamina intact. Bar, 0.1 μm. × 88,959.

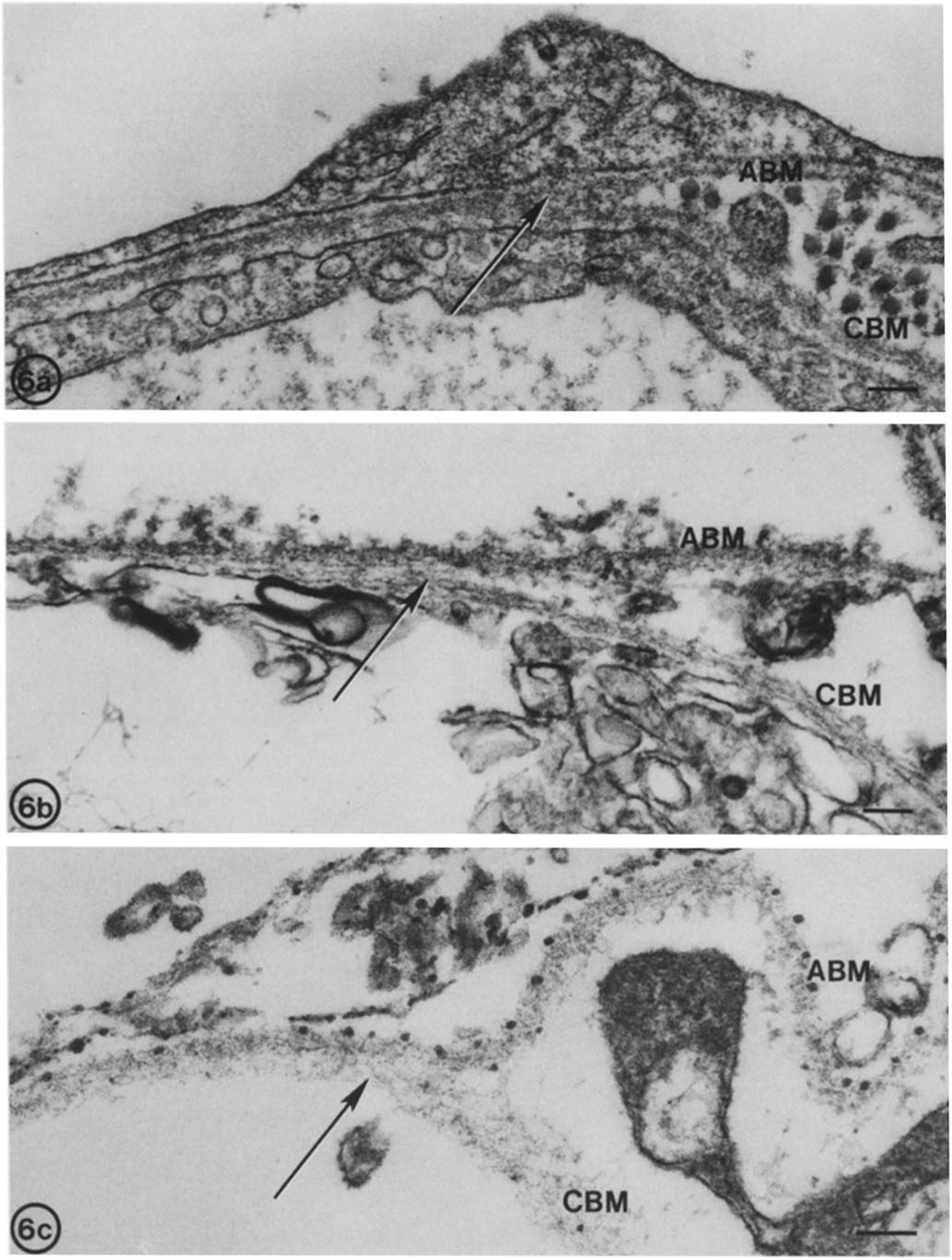

FIGURE 6 (*a*) In tannic acid-fixed specimens, fusions between the alveolar and the capillary basement membrane involve the focal coalescence of the lamina densa regions (arrow), which ultimately thin into a single basement membrane. Bar, 0.1 μm. × 92,858. (*b*) After treatment with guanidine hydrochloride, the CBM is more fibrillar, fusions remain intact (arrow), and thin until only amorphous ABM is visible. Bar, 0.1 μm. × 92,858. (*c*) The distribution of anionic sites and points of fusion (arrow) remains unchanged in tissue incubated with Triton X-100 and stained with ruthenium red. Bar, 0.1 μm. × 109,725.

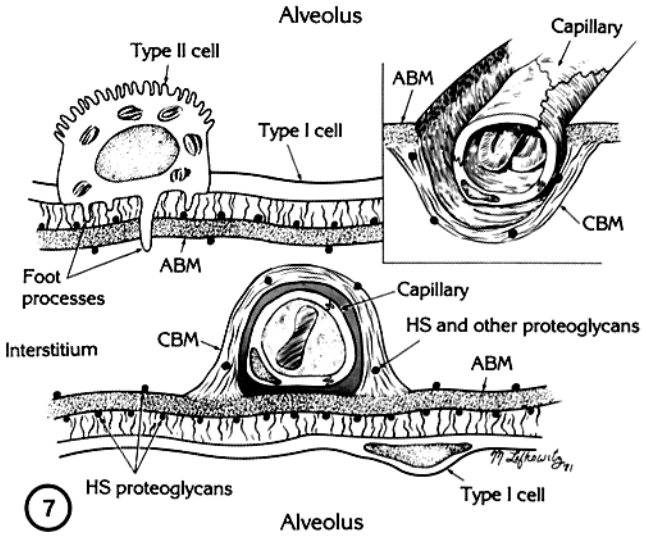

FIGURE 7 Schematic showing basement membrane organization of the alveolar wall in cross section and three-dimensional view of capillary enclosed by capillary basement membrane (*CBM*) in *inset*. Structures are not drawn to scale. Cells and connective tissue constituents of the interstitial space are not shown. Fine filaments and heparan sulfate (*HS*) proteoglycans are associated with the luminal surface of the lamina densa of the alveolar basement membrane (*ABM*). The ABM has a dense amorphous appearance, whereas the CBM is more loose and fibrillar. HS and other proteoglycans appear on all surfaces of the CBM. Alveolar type II cells have basilar foot processes, some of which penetrate the ABM lamina densa. The CBM (shown in *inset*) holds the capillary in a slinglike fashion against the ABM, forming focal fusions on either side of the capillary. The CBM compartmentalizes the alveolar wall into a thin gas-exchange side and a thick interstitial side.

to the organization, distribution, and type of proteoglycan within each basement membrane. The nature of these macromolecules is demonstrated by their anionic nature, as revealed by staining with the cationic dye ruthenium red, and by their selective degradation by crude heparanase and/or chrondroitinase ABC. Alveolar basement-membrane anionic sites appear to be exclusively heparan sulfate proteoglycans, whereas the CBM sites appear to be a mixture of heparan sulfate and other chondroitinase-sensitive proteoglycans. Heparan sulfate proteoglycans appear in a linear array in the laminae rarae of the ABM, with a distinct predominance on tbe luminal side of the ABM. Their organization is similar to the regular lattice of heparan sulfate proteoglycans noted by Gordon and Bernfield (39) in basement membrane of mammary epithelium. Their spacing approximates the 70-nm spacing noted by those authors, suggesting similar organization of proteoglycans in at least some epithelial basement membranes. In contrast, proteoglycans appear to be embedded within and on the surface of the lamina densa of the CBM. Further, morphometric analysis of the anionic sites suggests that ABM contains several times the amount of ruthenium red–reactive proteoglycan that CBM contains. It is of interest that glomerular basement membranes have the same distribution of heparan sulfate proteoglycans with predominance in the lamina rara externa as we have shown with ABM (20).

The function of the basement-membrane-associated proteoglycans in the adult lung is unclear. Several investigators have detailed the importance of heparan sulfate proteoglycans in regulating the permeability of the glomerular basement membranes to proteins (40). The highly anionic proteoglycans establish a charge-dependent filtering barrier that prevents protein from appearing in the glomerular filtrate under normal circumstances. The lung basement-membrane-associated proteoglycans might serve a similar purpose. Studies of proteins appearing in lung lymph, draining from the alveolar interstitium, have shown that molecular size is not the only factor that controls filtration of macromolecules in the pulmonary capillaries (41). Further, capillary endothelium is more permeable to macromolecules than alveolar epithelium (41). Although difference in permeability has been attributed to differences in endothelial and epithelial cell junctions (42), the greater density of proteoglycans on ABM vs. CBM or the difference in their distribution may also play a role in regulating pulmonary permeability. It is also possible that the above-noted differences in structure of ABM and CBM lamina densa may affect this process. Loss of heparan sulfate proteoglycans from glomerular capillaries in immune disease (43), in experimental nephrosis (44), or induced by perfusion with heparinase allows movement of protein into the urine (45). It is possible that a similar loss of the proteoglycan filtering mechanism is involved in forms of permeability or noncardiogenic pulmonary edema. The basement-membrane-associated proteoglycans may serve other purposes that explain differences in ABM and CBM distribution. Proteoglycans have been implicated in the process of cell attachment (46, 47). Their luminal predominance on ABM may serve to regulate the basement-membrane scaffold function described by Vracko (2). Proteoglycans may also influence cell renewal during periods of accelerated lung growth or during lung repair after injury.

Our studies have clearly indicated that ABM and CBM fuse in a focal fashion, leaving the ABM as the single structure separating epithelium and endothelium on the thin side of the alveolar wall. The single basement membrane separating capillary blood from alveolar air provides the thinnest possible barrier to gas diffusion in the lung. It also interposes the permeability characteristics of the ABM over the gas-exchange surface. In pulmonary edema, fluid has been shown to accumulate in the alveolar interstitium (i.e., on the thick side of the alveolus) but not on the thin side which contains the dense, highly anionic ABM, thus preserving the integrity of the gas-exchange surface until actual alveolar flooding occurs (48).

As noted in Fig. 7, the CBM appears to hold the capillary against the ABM in a slinglike fashion, providing a structural explanation for mechanical interdependence of capillary and alveolus (49). This structural sling that fixes the capillary in place may provide an explanation for the inability of the mature lung to form new alveoli. Alveolar formation is a complex, as yet incompletely understood anatomic event that appears to be associated with capillary proliferation (50). Most authors have felt that alveolar formation occurs exclusively during the early postnatal period and that the adult lung is incapable of forming new alveoli (51). We have found that the CBM is incomplete during the postnatal period of alveolar formation in the rat (52). As alveolar formation ceases, the CBM assumes its adult "locked in place" structure, perhaps preventing new capillary budding and new alveolar formation from occurring.

The mechanism by which CBM-ABM fusions evolve is unclear. There are no demonstrable unique features of the fusion site that provide insight into its structure. The CBM may never be produced on the side of the capillary adjacent to the ABM, or it may form but not stabilize and be subsequently degraded. Our observations of focal rather than continuous

fusion of CBM and ABM contrast with previous concepts of alveolar wall ultrastructure (8, 9, 12). Most prior studies have examined collapsed rather than inflated specimens, without special stains that highlight basement membrane, or have used aged or diseased lungs. We have noted increased deposition of CBM along the thin side of the alveolus in rats with bleomycin-induced pulmonary fibrosis and in old (27-mo) rats, suggesting that these factors may explain previous observations (53).

In summary, we have found a series of ultrastructural differences between ABM and CBM in the adult lung. Although the link between these structural characteristics and function has not been established, several possible consequences of our findings have been discussed. The well-known differences between capillary and alveolar permeability may be explained in part by the loosely organized nature of the CBM, which contains few heparan sulfate proteoglycan anionic sites. The luminal arrangement of heparan sulfate proteoglycans in the lamina rara of tbe ABM and the similar appearance of fine filaments may serve as attachment sites for alveolar epithelial cells during lung growth and repair. The discontinuities in ABM below alveolar type II cells that allow cytoplasmic processes of these cells to extend into the interstitium may provide a means of epithelial-mesenchymal interaction necessary for epithelial cytodifferentiation. Finally, the slinglike arrangement of CBM that fixes the capillary in place against the alveolar epithelium not only establishes a maximally efficient gas-exchange surface but compartmentalizes the tissues of the alveolar wall and may explain the inability of the adult lung to form new alveoli.

We thank Nancy Roth and Peggy Gill for their excellent technical assistance.

This work was supported by National Heart, Lung, and Blood Institute grant HL-19717.

Received for publication 6 April 1981, and in revised form 29 June 1981.

REFERENCES

1. Bernfield, M. R., and S. D. Banerjee. 1978. The basal lamina in epithelial-mesenchymal morphogenetic interactions. *In* Biology and Chemistry of Basement Membranes. N. A. Kefalides, editor. Academic Press, Inc., New York. 137–148.
2. Vracko, R. 1974. Basal lamina scaffold: anatomy and significance for maintainance of orderly tissue structure. *Am. J. Pathol.* 77:314–346.
3. Farquhar, M. G. 1978. Role of the basement membrane in glomerular filtration. *In* Biology and Chemistry of Basement Membranes. N. A. Kefalides, editor. Academic Press, Inc., New York. 43–80.
4. Liotta, L. A., K. Tryggvason, S. Garbisa, I. Hart, C. M. Foltz, and S. Shafie. 1980. Metastatic potential correlates with enzymatic degradation of basement membrane collagen. *Nature (Lond.).* 284:67–68.
5. Low, F. N. 1953. The pulmonary alveolar epithelium of laboratory mammals and man. *Anat. Rec.* 17:241–264.
6. Karrer, H. E. 1956. The ultrastructure of mouse lung. General architecture of capillary and alveolar walls. *J. Biophys. Biochem. Cytol.* 2:241–251.
7. Karrer, H. E. 1956. The ultrastructure of mouse lung. Some remarks regarding the fine structure of the alveolar basement membrane. *J. Biophys. Biochem. Cytol.* 2:287–289.
8. Low, F. N. 1961. The extracellular portion of the human blood-air barrier and its relation to tissue space. *Anat. Rec.* 139:105–111.
9. Ryan, S. F. 1969. The structure of the interalveolar septum of the mammalian lung. *Anat. Rec.* 165:467–484.
10. Madri, J. A., and H. Furthmayr. 1980. Collagen polymorphism in the lung. *Hum. Pathol.* 11:353–365.
11. Weibel, E. R. 1973. Morphologic basis of alveolar-capillary gas exchange. *Physiol. Rev.* 53:419–495.
12. Huang, T. W. 1978. Composite epithelial and endothelial basal laminas in human lungs. *Am. J. Pathol.* 93:681–687.
13. Vaccaro, C. A., and J. S. Brody. 1979. Ultrastructural localization and characterization of proteoglycans in the pulmonary alveolus. *Am. Rev. Respir. Dis.* 120:901–910.
14. Sergio, B. A., and V. Tsutsmi. 1970. A fast method for processing biologic material for electron microscopy. *Lab. Invest.* 23:447–450.
15. Karnovsky, M. J. 1965. A formaldehyde-glutaraldehyde fixative of high osmolality for use in electron microscopy. *J. Cell Biol.* 27:137–138.
16. Yamagata, T., S. Hidehiko, O. Habuchi, and S. Sakarv. 1968. Purification and properties of bacterial chondroitinase and chondrosulfatase. *J. Biol. Chem.* 243:1523–1535.
17. Gill, P. J., J. Adler, C. Silbert, and J. Silbert. 1981. Removal of glycosaminoglycans from cultures of human skin fibroblasts. *Biochem. J.* 194:299–307.
18. Klebe, R. J., K. L. Bently, P. J. Sasser, and R. C. Schoen. 1980. Elution of fibronectin from collagen with chaotropic agents. *Exp. Cell Res.* 130:111–117.
19. Kefalides, N. A. 1978. Current status of chemistry and structure of basement membranes. *In* Biology and Chemistry of Basement Membranes. N. A. Kefalides, editor. Academic Press, Inc., New York. 215–228.
20. Kanwar, Y. S., and M. G. Farquhar. 1979. Anionic sites in the glomerular basement membrane. *J. Cell Biol.* 81:137–153.
21. Kanwar, Y. S., and M. G. Farquhar. 1980. Detachment of endothelium and epithelium from the glomerular basement membrane produced by kidney perfusion with neuraminidase. *Lab. Invest.* 42:375–384.
22. Stenman, S., and Vaheri, A. 1978. Distribution of a major connective tissue protein, fibronectin, in normal human tissues. *J. Exp. Med.* 147:1054–1064.
23. Perkins, M. E., T. H. Ji, and R. O. Hynes. 1979. Cross-linking of fibronectin to sulfated proteoglycans at the cell surface. *Cell.* 16:941–952.
24. Yamada, K. M., D. W. Kennedy, K. Kimata, and R. M. Pratt. 1980. Characterization of fibronectin interactions with glycosaminoglycans and identification of active proteolytic fragments. *J. Biol. Chem.* 255:6055–6063.
25. Foidart, J. M., E. W. Bere, Jr., M. Yaar, S. I. Rennard, M. Gullino, G. R. Martin, and S. I. Katz. 1980. Distribution and immunoelectron microscopic localization of laminin, a non-collagenous basement membrane glycoprotein. *Lab. Invest.* 42:336–342.
26. Madri, J. A., F. J. Roll, H. Furthmayr, and J. M. Foidart. 1980. Ultrastructural localization of fibronectin and laminin in the basement membranes of the murine kidney. *J. Cell Biol.* 86:682–687.
27. Singley, C. T., and M. Solursh. 1980. The use of tannic acid for the ultrastructural visualization of hyaluronic acid. *Histochemistry.* 95:93–102.
28. Weibel, E. R., P. Gehr, D. Haies, J. Gil, and M. Bachofen. 1976. The cell population of the normal lung. *In* Lung Cells in Disease. A. Bouhuys, editor. Elsevier/North-Holland Inc., New York. 3–16.
29. Cutler, L. S., and A. P. Chaudhry. 1973. Intercellular contacts at the epithelial/mesenchymal interface during the prenatal development of the rat submandibular gland. *Dev. Biol.* 33:229–240.
30. Bluemink, J. G., P. V. Maurik, and K. A. Lawson. 1976. Intimate cell contacts at the epithelial/mesenchymal interface in embryonic mouse lung. *J. Ultrastruct. Res.* 55:247–270.
31. Bride, J., and L. Gomot. 1978. Changes at the ecto-mesodermal interface during development of the duck preen gland. *Cell Tissue Res.* 194:141–9.
32. Saxén, L., and E. Lehtonen. 1978. Transfilter induction of kidney tubules as a function of the extent and duration of intercellular contacts. *J. Embryol. Exp. Morphol.* 47:97–109.
33. Evans, M. J., L. J. Cabral, R. J. Stephens, and G. Freman. 1975. Trasnformation of alveolar type 2 cells to type 1 cells following exposure to NO_2. *Exp. Mol. Pathol.* 22:142–150.
34. Brody, J. S., R. Burki, and N. Kaplan. 1978. Deoxyribonucleic acid synthesis in lung cells during compensatory lung growth after pneumonectomy. *Am. Rev. Respir. Dis.* 117:307–316.
35. Smith, B. T. 1979. Lung maturation in the fetal rat: acceleration by injection of fibroblast-pneumonocyte factor. *Science (Wash. D. C.).* 204:1094–1095.
36. Smith, B. T., W. Galaugher, and W. M. Thurlbeck. 1980. Serum from pneumonectomized rabbits stimulates alveolar type II cell proliferation in vitro. *Am. Rev. Respir. Dis.* 121:701–707.
37. Smith, L. J., and J. S. Brody. 1981. Influence of corticosteroids on mouse alveolar type 2 cell response to acute lung injury. *Am. Rev. Respir. Dis.* 123:459–464.
38. Dobbs, L. G., and R. J. Mason. 1979. Pulmonary alveolar type II cells isolated from rats. Release of phosphatidylcholine in response to adrenergic stimulation. *J. Clin. Invest.* 63: 378–387.
39. Gordon, J., and M. R. Bernfield. 1980. The basal lamina of the postnatal mammary epithelium contains glycosaminoglycans in a precise ultrastructural organization. *Dev. Biol.* 74:118–135.
40. Brenner, B. M., T. H. Hostetter, and H. D. Humes. 1978. Molecular basis or proteinuria of glomerular origin. *N. Engl. J. Med.* 298:826–833.
41. Brigham, K. L. 1977. Factors affecting lung vascular permeability. *Am. Rev. Respir. Dis.* 115(Pt. 2):165–172.
42. Schneeberger, E. E., and M. J. Karnovsky. 1976. Substructure of intercellular junctions in freeze-fractured alveolar-capillary membranes of mouse lung. *Circ. Res.* 38:404–411.
43. Kelley, V. A., and T. Cavallo. 1980. Glomerular permeability. Focal loss of anionic sites in glomeruli of proteinuric mice with lupus nephritis. *Lab. Invest.* 42:59–64.
44. Caufield, J. P. 1979. Alterations in the distribution of Alcian blue staining fibrillar anionic sites in the glomerular basement membrane in aminonucleoside nephrosis. *Lab. Invest.* 40:503–511.
45. Kanwar, Y. S., A. Linker, and M. G. Farquhar. 1980. Increased permeability of the glomerular basement membrane to ferritin after removal of glycosaminoglycans (heparan sulfate) by enzyme digestion. *J. Cell Biol.* 86:688–693.
46. Culp, L. A., R. J. Rollins, J. Buniel, and S. Hitri. 1978. Two functionally distinct pools of glycosaminoglycan in the substrate adhesion site of murine cells. *J. Cell Biol.* 79:788–801.
47. Schubert, D., and M. La Corbière. 1980. A role of secreted glycosaminoglycans in cell-substratum adhesion. *J. Biol. Chem.* 255:11564–11569.
48. Cottrell, T. S., G. R. Levine, R. M. Senior, J. Weiner, D. Spiro, and A. P. Fishman. 1967. Electron microscopic alterations at the alveolar level in pulmonary edema. *Circ. Res.* 21: 783–797.
49. Benjamin, J. J., P. S. Murtagh, D. F. Procor, H. A. Menkes, and S. Permutt. 1974. Pulmonary vascular interdependence in excised dog lobes. *J. Appl. Physiol.* 37:887–894.
50. Burri, P. H. 1974. The postnatal growth of the rat lung. III. Morphology. *Anat. Rec.* 180: 77–98.
51. Thurlbeck, W. M. 1975. Postnatal growth and development of the lung. *Am. Rev. Respir. Dis.* 111:803–844.
52. Brody, J. S., and C. A. Vaccaro. 1981. Alterations in alveolar and capillary basement membranes during postnatal lung growth in the rat. *Am. Rev. Respir. Dis.* 123(pt.2):239 (Abstr.).
53. Vaccaro, C. A., and J. S. Brody. 1981. Alveolar and capillary basement membrane in normal and fibrotic rat lungs. *Fed. Proc.* 40:792.